Title

Spectroscopic Characterization of μ-η1:η1-Peroxo Ligands Formed by Reaction of Dioxygen with Electron-Rich Iridium Clusters

Journal

Inorganic Chemistry, 58(21)

ISSN

0020-1669

Authors

Palermo, Andrew P
Schöttle, Christian
Zhang, Shengjie
et al.

Publication Date

2019-11-04

DOI

10.1021/acs.inorgchem.9b01529

Peer reviewed

Dioxygen Reacts on a Silica-Supported Tetrairidium Cluster to Form μ-η^1:η^1-Peroxo Ligands

Andrew P. Palermo[a], Christian Schöttle[b], Shengjie Zhang[c], Nicolás Grosso-Giordano,[b] Alexander Okrut,[b] David A. Dixon[c]*, Heinz Frei[d]*, Bruce C. Gates[a]*, Alexander Katz[b]*

Although oxygen is a common ligand in supported-metal catalysts, its coordination has been challenging to elucidate. Using a well-defined Ir-dimer cluster that incorporates a μ-η^1:η^1-peroxo ligand, we observe a FT-Raman band at 756 cm^{-1} assigned to the ^{16}O–^{16}O stretch, and a greatly enhanced intensity at 788 cm^{-1}. The frequency of this latter band does not change upon ^{18}O labeling, suggesting it arises due to a change in symmetry accompanying bridging peroxo-ligand incorporation. We also investigate reaction of oxygen with a silica-supported tetrairidium carbonyl cluster protected with bulky electron-donating phosphine ligands (*p-tert*-butyl-calix[4]arene(OPr)$_3$(OCH_2PPh_2; Ph = phenyl; Pr = propyl), and observe the same Raman band at 788 cm^{-1}, which is associated with formation of similar bridging peroxo ligands on the tetrairidum frame. IR spectra recorded as the supported cluster was decarbonylated in sequential exposures to (i) H_2, (ii) O_2, (iii) H_2, and (iv) CO are consistent with two bridging peroxo ligands bonded irreversibly per supported tetrairidium cluster, replacing bridging carbonyl ligands, without altering either the cluster frame or bound phosphine ligands. X-ray absorption near edge and infrared spectra recorded as the cluster reacted with O_2 include isosbestic points signifying a stoichiometrically simple reaction, and mass spectra of the effluent gas identify CO_2 formed by oxidation of one terminal CO ligand per cluster and H_2 (not H_2O)—evidence that hydride ligands had been present on the cluster. The results demonstrate that O_2 reacts with intact ligated metal polyhedra on supports—an inference that pertains broadly to oxidation catalysis on supported noble metals.

Oxygen is a ubiquitous ligand in metal complexes, playing key roles in catalysis.[1] The chemistry is nuanced and complex because of the multiplicity of configurations of metal-oxygen bonding, controlled by both charge and coordination geometry, as illustrated, for example, by compounds with peroxo and superoxo ligands on metal sites—that is, ligands bonded as (η^1, η^2, μ^1-η^1:η^1, etc. species).[2–4] Many of the reported compounds are mononuclear complexes of Group 9 transition metals.[5–11] When the metals are anchored on solid surfaces, the complexity of the structures involving metal-oxygen bonding is typically greater than that in molecular species, because of the multiple metal centers involved, with additional complexity associated with oxide-support surface heterogeneity and interactions and possible surface distortion by ligated oxygen.[12–17] An improved understanding of supported structures comprising metal-metal and metal-oxygen bonds is crucial for the prediction of structure-function relationships and is essential for design of solid noble-metal catalysts.[18–23]

Our goals in the current work were to better understand metal-oxygen bonding in a supported species that incorporates metal-metal bonds. We used as a starting point for our investigation the tetrahedral Ir_4 framework of metal cluster **1**, which is stabilized by three bulky electron-donor phosphine *tert*-butyl-calix[4]arene(OPr)$_3$(OCH_2PPh_2) (Ph = phenyl; Pr = propyl) ligands, in addition to six terminal and three bridging carbonyl ligands. This cluster has been fully characterized structurally, as reported elsewhere.[24,25] A unique opportunity afforded by the supported clusters was to investigate their reactions with various ligands presented as gas-phase reactants in flowing streams, so that even ligands more weakly bound than those initially present could become bonded to the metal as the flowing gas swept away desorbed ligands even when they were present in low concentrations. With such clusters on the surface of silica, we characterized the loss of CO in helium and hydrogen atmospheres, characterizing the activation of hydrogen on the cluster surface and contrasting the chemistry of the cluster in alkane solvent and on the support.[26]

To understand the interactions of oxygen with Ir atoms of the supported cluster frame, we used complementary spectroscopic methods and leveraged the earlier work on

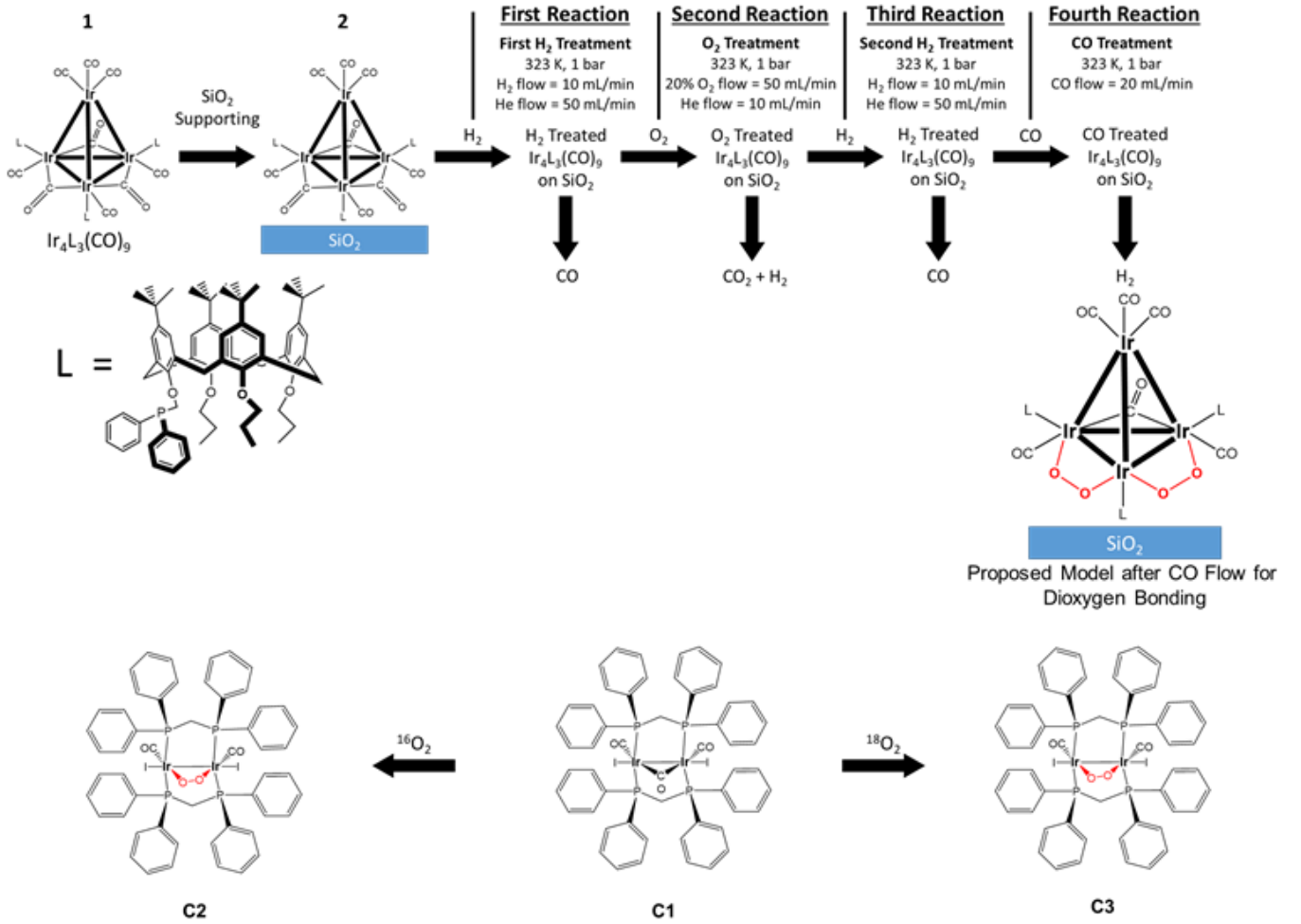

Figure 1. Top panel: Schematic representation of the sequence of gas treatments used to characterize the bonding of oxygen to the supported Ir_4 framework of **2**. The horizontal arrows designate the gas to which the sample was exposed. The vertical arrows show the gases that were formed as products when the treatment gas was the one shown at the immediate left. Each treatment was performed in a flow system at 323 K and 1 bar as IR spectra of the solid sample were recorded and as the effluent gases were characterized by mass spectrometry. Bottom panel: Reaction of dioxygen with clusters **C1** and **C2** previously synthesized and characterized by single-crystal X-ray diffraction by Cowie et al.[27,28]

supported cluster **1** (represented by **2**).[26] Given that thoroughly characterized compounds incorporating bridging peroxo ligands are largely restricted to dimers of first-row transition metals (although metal "oxo-peroxo" clusters have been reported),[29–37] and the greatly varied forms of oxygen as a ligand in general,[2] we wished to investigate how oxygen would bond to our supported cluster. We do so by reacting O_2 in the presence of other ligands that include the silica support, and elucidate how its bonding influences ν_{CO} bands in the infrared (IR) spectrum of our supported cluster. Here, we thus investigated the reactions of supported cluster **2** during sequential treatments involving H_2, O_2, and CO. To characterize the oxygen ligands that formed during reaction with O_2, we turned to previously reported clusters **C1** and **C2** (and newly synthesized ^{18}O-labeled **C3**), the latter of which is synthesized by simply exposing a solution of the former to atmospheric oxygen. Cluster **C2** thus serves as a standard, as the first reported iridium cluster that incorporates a bridging peroxo ligand; it has been characterized by single-crystal X-ray diffraction crystallography by Cowie et al.[27] The results include the first vibrational spectra characterizing a bridging peroxo ligand involving iridium and the first bridging peroxo ligand on a intact supported metal cluster.[29,36]

Results

Reactions of supported tetrairidium clusters with H_2, O_2, and CO: characterization of clusters with IR spectroscopy and identification of evolved gases by mass spectrometry

We investigated the sequential reactions of silica-supported cluster **2** with H_2, O_2, and CO at 323 K and 1 bar, as outlined in Figure 1, using *in-situ* IR spectroscopy to characterize the bonding of the ligands to the iridium centers and mass spectrometry to identify the evolved gases. In earlier work,[26,38] it was shown that during exposure of the silica-supported cluster $Ir_4L_3(CO)_9$ to H_2 at 323 K, as many as one terminal and two bridging CO ligands were removed per cluster, all at the basal plane, by a process that was controlled by the rate of CO dissociation. Isosbestic points observed during this treatment demonstrate a stoichiometrically simple transformation (Figures 2a and S1 and S2 in the Electronic Supporting Information

(ESI)). The data of Figures 2a and b demonstrate that the bands representing terminal CO ligands, at 2046 and 1994 cm^{-1}, were shifted to 2053 and 2011 cm^{-1}, respectively. These blue shifts were accompanied by formation of new Ir-H band at 2110 cm^{-1}, as a result of the oxidative addition of hydrogen to the metal.

The resulting electron-rich phosphine-functionalized clusters incorporating reactive hydride ligands offered an opportunity to investigate reactions with O_2,[39,40] which in our experiments flowed over and through the powder sample in the IR cell. During this treatment, we observed a slight decrease in intensity in the terminal carbonyl region, signifying the removal of an additional terminal CO ligand, quantified by measurement of the peak area (Table 1). Furthermore, during reaction of the H_2-treated sample with O_2, the blue shift of the terminal carbonyls characterized by bands at 2053 and 2011 cm^{-1} (observed during the initial reaction of **2** with H_2) caused these bands to revert to their original frequencies, corresponding to those in **2**. Simultaneously, characteristic metal-hydride bands at 2110 cm^{-1} disappeared. Characteristic times for this process were found to be 27 ± 1 min, as shown in Figures S3 and S4 of the ESI. The presence of isosbestic points in Figures 1a and S1b of the ESI indicates a stoichiometric change occurring as the supported tetrairidium clusters that formed during reaction with H_2 were subsequently converted to a new species after reaction with O_2 (second reaction of Figure 1).

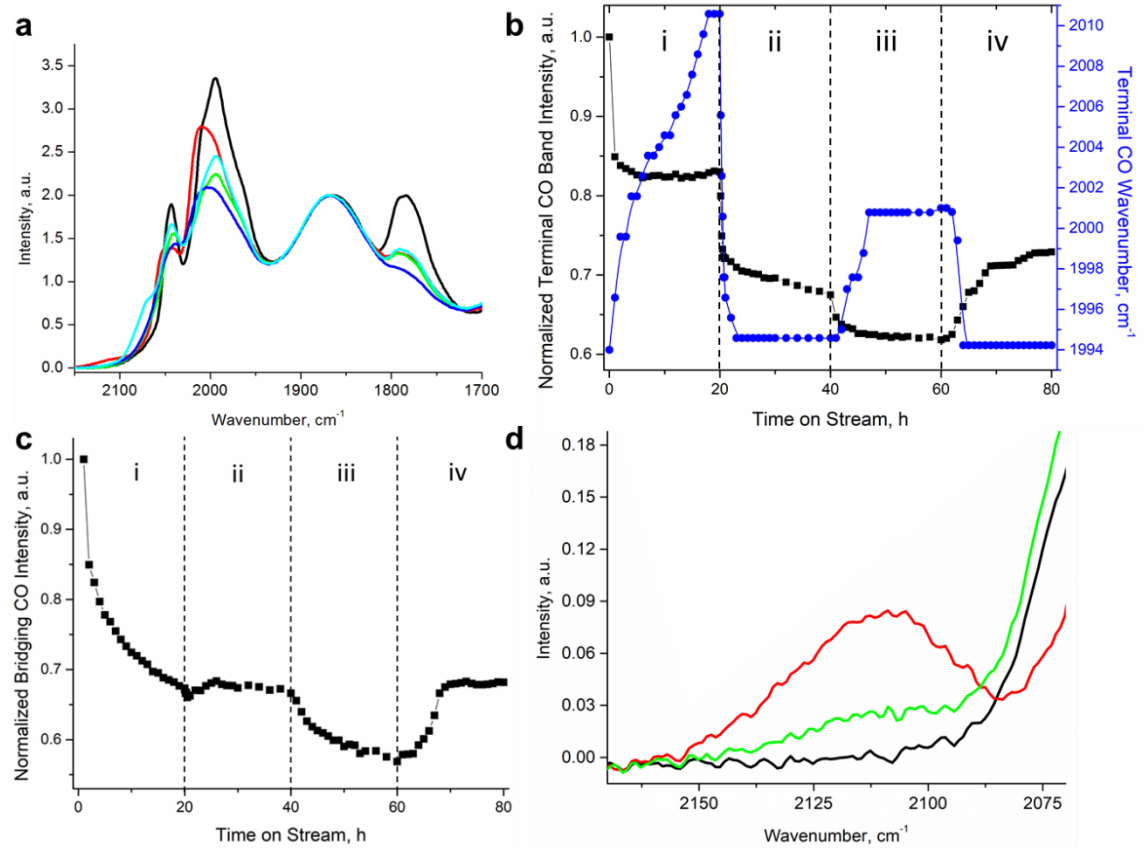

Figure 2. (a) IR spectra in the ν_{CO} stretching region characterizing SiO_2-supported clusters initially present as $Ir_4L_3(CO)_9$ (black) during the following sequential treatments: first, in flowing H_2 (red), then flowing O_2 (green), then, again, flowing H_2 (dark blue), and then flowing CO (light blue). (b) IR terminal carbonyl band intensity (black squares) and wavenumber (blue circles). (c)I Intensity of bridging carbonyl band plotted as a function of time on stream during (i) exposure to H_2 (in the flow system), (ii) subsequent exposure to O_2, (iii) the second (subsequent) exposure to H_2, and (iv) recarbonylation by exposure to CO. (d) Difference IR spectra in the metal-hydride stretching region during the first exposure to H_2 (red), then followed by exposure to O_2 (black), and then followed by exposure again to H_2 (green). Spectra are difference spectra determined by subtracting from each observed spectrum the spectrum of the original SiO_2-supported $Ir_4L_3(CO)_9$ at 323 K and 1 bar. The conditions were as follows: the first exposure to H_2 (flowing at a rate of 10 mL(NTP)/min with helium flowing at a rate of 50 mL(NTP)/min); then exposure to O_2 (flowing at a rate of 60 mL(NTP)/min in a stream consisting of 17% O_2 and the balance helium); and then the second exposure to H_2 (flowing at a rate of 10 mL(NTP)/min with helium flowing at a rate of 50 mL(NTP)/min); followed by exposure to CO flowing at a rate of 20 mL(NTP)/min.

Table 1. Changes in carbonyl band intensities resulting from the various reactions of the supported clusters

Supported Cluster	Terminal CO band area, a.u.	Bridging CO band area, a.u.	Number of terminal CO ligands lost per cluster[i]	Number of bridging CO ligands lost per cluster[i]
$Ir_4L_3(CO)_9/SiO_2$	139	64.9	0	0
Preceding cluster after exposure to H_2	117	27.3	1.04	1.74
Preceding cluster after exposure to O_2	94.6	23.3	1.76	1.92
Preceding cluster after exposure to H_2	90.9	14.9	2.48	2.63
Preceding cluster after exposure to CO	112	22.9	0.98	2.13

i. Quantification of carbonyl ligands was done by integration of either terminal or bridging carbonyl bands.

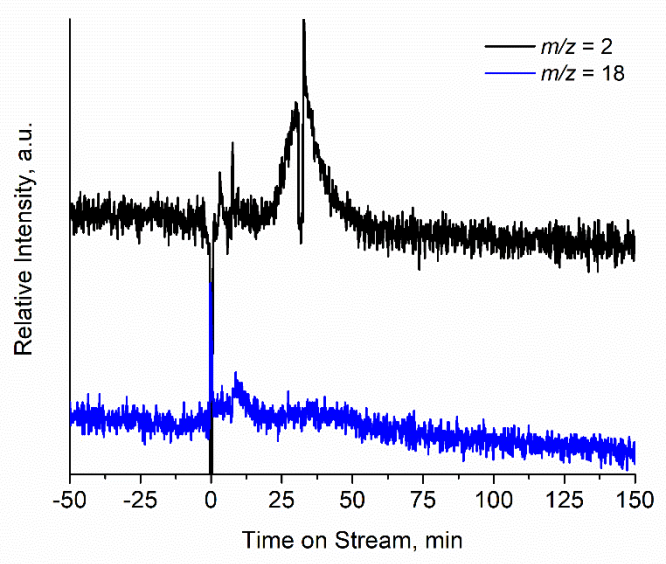

Figure 3. Raw mass spectrometry signals for *m/z* = 2 and 18 as a function of time on stream during exposure to O_2 at 323 K of the supported clusters that had been previously treated for 20 h with H_2. Spikes at 0 and 31 min represent the gas switch from He to O_2 and a reactor bypass, respectively. The drop *m/z* = 2 intensity at 31 min demonstrates that the signal this signal characterizing H_2 off-gas originates from the catalyst in the reactor and not an artefact from the flow system.

There was no observable change in the number of silanols on the silica support (indicated by the spectra in the ν_{OH} stretching region) during the reaction of the sample with O_2 (Figure S5 in the ESI). Mass spectra of the effluent gas (Figures 3 and S6 in the ESI) show that no water formed in the reaction with O_2. As the sample was heated to 323 K during the reaction in flowing O_2, the *m/z* signals 2 and 44 increased in intensity, demonstrating that H_2 (Figure 3) and CO_2 (Figure S6, ESI) were evolved during the treatment. Infrared spectroscopic data in the expected frequency range corresponding to bound carbonate ligands[41] demonstrates no detectable carbonato complexes formed during reaction with dioxygen (Figure S15, ESI). Confirmation that the effluent products arose directly from reaction of the supported clusters was provided by the results of experiments carried out with a bypass of the flow reactor (Figure 3 at 30 min)—then, only the reactant O_2 in the feed stream was observed in the effluent. The mass spectra show that no water was present in the effluent stream when the supported cluster that had been exposed to H_2 was later exposed to O_2, demonstrating that O_2 did not react with hydride ligands on the clusters to give water.

In experiments carried out to investigate whether the cluster-bound oxygen species would react with H_2, the supported clusters that had reacted first with H_2 and then with O_2 were exposed a second time to flowing H_2, followed by a final treatment consisting of exposure to flowing CO. The goal of the last of the treatments was to determine whether the clusters would be recarbonylated after incorporation of any hydride ligands that might have been bonded to the cluster as a result of the second exposure to H_2. The second exposure to H_2 led to the reappearance of the aforementioned Ir-H band in the IR spectrum, at the same frequency as was observed during the first hydrogen exposure.

The carbonyl band initially at 1994 cm^{-1} was blue shifted 7 cm^{-1} after the second exposure to H_2 (i.e., the third reaction in Figure 1) as hydride ligands formed. This blue shift was quickly and completely reversed (giving a spectrum with carbonyl band frequencies identical to those of **2**) when the sample was subsequently exposed to CO (Figure S1 in the ESI). However, the CO band observed initially for **2** at 2046 cm^{-1} did not shift during the second exposure (after O_2 exposure) of the sample to H_2 (Figure S1 in the ESI). In both the first and second reactions of the supported cluster with flowing H_2, a blue shift was observed, but the extent of the blue shifts was not the same. The hydride band intensity and the magnitude of the blue shift were reduced by nearly 66% during the second exposure to H_2 relative to the first. These data clearly demonstrate that new ligands formed on the supported clusters as they reacted with O_2; we return below to this point and identification of the oxygen-containing ligands. Isosbestic points in the IR spectra of Figure 2a show that the changes undergone by the clusters during the partial recarbonylation are the result of a stoichiometrically simple reaction.

Quantitative information characterizing the changes in the clusters that had undergone exposure of silica-supported cluster **2** to H_2, then O_2, and then H_2 again was obtained by measuring difference IR spectra, shown in Figure 2d. The absorbance of the hydride band at 2110 cm^{-1} following the first exposure of the clusters to H_2 was 0.084 a.u., and

this band became undetectable after subsequent exposure to O_2. During the second period of exposure to H_2, the band reappeared at the same frequency but with a significantly lower absorbance, 0.029 a.u. The data are shown in Figure 2d.

Taking the quantitative data together (Figures 2 and S8 in the ESI and Table 1), we infer that the exposure of the sample to CO following the exposures to H_2, then O_2, and then H_2 again led to recarbonylation to the extent of nearly 1.5 terminal and 0.5 bridging carbonyl ligands per cluster, with one terminal and two bridging carbonyl ligands that were initially present not replaced upon the final CO exposure.

Formation of oxygen-containing ligands on the clusters indicated by Raman Spectroscopy

Raman data characterizing **C1**, **C2**, and **C3** in the frequency range predicted for O-O stretching by electronic structure calculations at the DFT level with various functionals (including the range 740–964 cm^{-1} for **C2** and **C3;** see Tables S1 and S2 in the ESI) are shown in Figures 1a and 1b, respectively. Comparing the effect of oxygen isotopic labelling, a broad Raman band centered at 756 cm^{-1} characterizing **C2** is evident in Figure 5b, and it is absent from the spectrum of **C3** in Figure 5c. This frequency is consistent with reported ^{16}O-^{16}O stretches in peroxo bands.[32–35,42] **C3** consists of a shoulder at 729 cm^{-1}, and a strong intensity gain at 701 cm^{-1}. This shoulder and strong intensity enhancement are not present in **C2**, and we infer that these are a consequence of ^{18}O-labeling, resulting in a mean frequency red shift of 41 cm^{-1} from the 756 cm^{-1} band, which coincides with DFT-calculated shifts based on a harmonic model with different functionals (Table S2, ESI). We thus assign the 756 cm^{-1} band to bridging peroxo O-O stretching vibrations in **C2**. The manifestation of the ^{18}O-shifted band from a single band at 756 cm^{-1} in **C2** to two normal vibrations in **C3** points to the fact that this O-O mode contributes to the potential energy distribution of two different normal modes. This effect may be caused by anharmonicty (i.e. Fermi resonance), although we can't rule out this being consistent with a purely harmonic model.

Next, we investigated the FT-Raman spectra of cluster **2**, both before and after treatment with flowing H_2 (20 h) and O_2 (20 h) at 50 °C. The data (Figures 5d and 5e, respectively) demonstrate the growth of a new Raman band in these treatments, at 788 ± 6 cm^{-1}. A noteworthy observation is that we observe the same band upon reaction of **C1** with both $^{16}O_2$ and $^{18}O_2$, in Figures 5b and 5c, respectively. Due to signal-to-noise limitations in Figure 5e, we are unable to assign a O-O stretching band for **2** following O_2 treatment.

Electronic structure calculations at the level of density functional theory were performed to better understand the structures containing bridging O_2 ligands. Calculations were done for **C2** and also for a tetrairidium core incorporating CO and phosphine ligands and two O_2 ligands replacing two bridging CO ligands in the basal plane (Scheme 1). The phosphine ligands were modelled as both $PMePh_2$ and PMe_3. The calculations were performed on four model structures comprising (i) terminal CO vacancy V in the apical and radial positions; (ii) an apical C_2H_5 (in place of V) and radial CO vacancy V; (iii) an apical C_2H_5 (in place of V) and a radial H (in place of V); and (iv) an H in the radial vacancy and a CO in the apical vacancy. For these structures, we used the wB97x-D functional, which includes Grimme's van der Waals correction. The O-O bond distances are predicted to be between 1.32 and 1.39 Å (see the ESI), with frequencies in the range of 930-1220 cm^{-1} for the O_2 stretches. These bond distances are consistent with an O_2^- moiety (optimized r = 1.349 Å, ν = 1229 cm^{-1}). The calculated O_2 stretching frequencies are too high relative to the experimental values. As noted previously, to provide more insight into these values, the structure and frequencies of **C2** were calculated with a range of functionals, as shown in the ESI. The O-O stretching frequency exhibits a high degree of sensitivity to the functional and to the O-O distance, with distance differences of less than 0.05 Å corresponding to differences of almost 200 cm^{-1} in the O-O stretching frequency. It is important in this context that the O-O distance was not exactly determined in the original crystal structure of **C2**[27] and that the remaining predicted geometry parameters are in good agreement with the experimental values of **C2**. This comparison shows that the calculations are highly sensitive to the degree of charge transfer between the Ir atom and the O_2 in our Ir_4 cluster. It is apparent that the calculations underestimate the amount of O_2^{2-} character. Subtle changes associated with the sizes of the ligands as well as any weak interactions with the support could conceivably impact the degree of charge transfer between the Ir atom and the O_2 ligands, which affects the value of the O_2 asymmetric stretch. We note that the current experimental value for the O_2 asymmetric stretch for our structure and for **C2** is consistent with Cowie et al.'s supposition that the O-O distance of 1.58 Å from the disordered crystal structure is too long[27], and that it is more likely to be near 1.50 Å. The terminal CO stretching frequencies range from 2025 to 2135 cm^{-1}, and the bridging CO stretching frequency ranges from 1660 to 1815 cm^{-1}, depending on the structure. Taken together, these results are consistent with the experimental values.

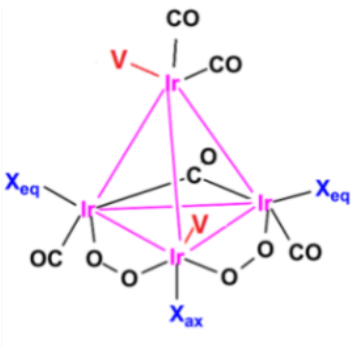

Scheme 1. Molecular model of tetrairidium cluster incorporating bridging dioxygen ligands used for electronic-structure calculations. CO vacancies are defined by V and were either left as vacancies or populated with ligands as described in the main text.

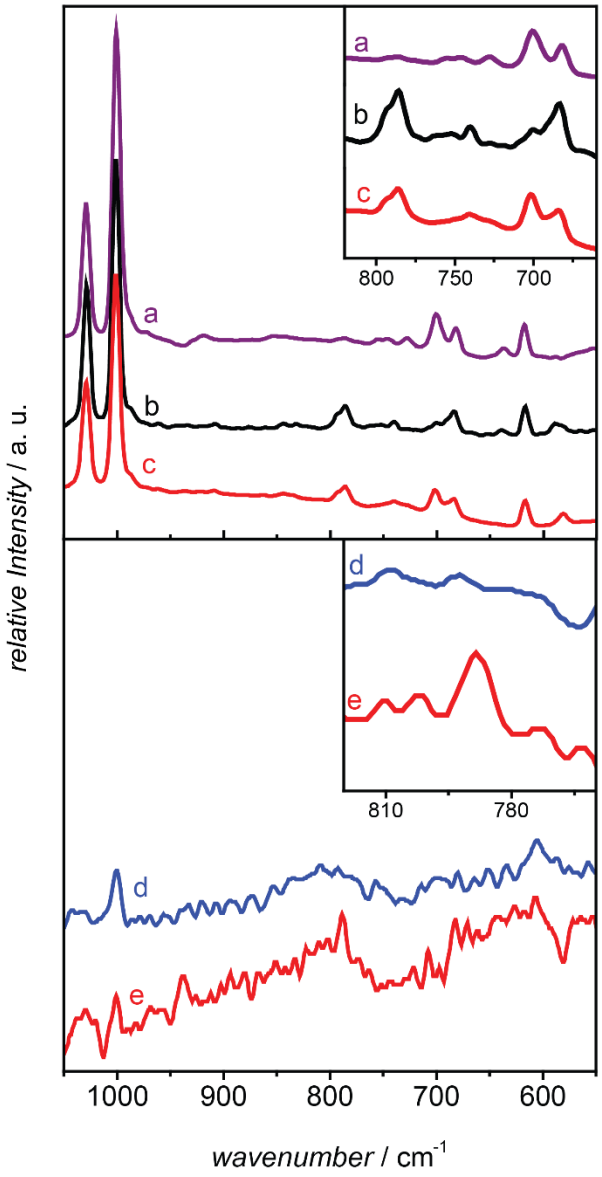

Figure 5. FT-Raman spectra a) **C1**; b) **C2** (synthesized by reaction of **C1** with $^{16}O_2$); c) **C3** (synthesized by reaction of **C1** with $^{18}O_2$); d) **2** (supported on silica with a loading of 2 wt. %); and e) **2** (supported on silica with a loading of 2 wt. %) after H_2 and O_2 gas-flow treatments described in the main text.

Confirmation of changes in the ligand sphere of iridium by X-ray absorption near edge spectroscopy

X-ray absorption near edge spectroscopy (XANES) at the Ir L_{III} edge was performed to provide further evidence of the changes in the supported clusters that incorporated hydride ligands as they were exposed to flowing O_2. The data of Figures S11a and S12 of the ESI demonstrate an increase in white-line intensity as O_2 reacted with the clusters. The data shown in the inset of Figure S11a in the ESI demonstrate that the edge energy decreased by 0.57 eV during reaction with O_2. Data in the XANES region (Figure S11a in the ESI) are characterized by two isosbestic points, which demonstrate that the reaction was stoichiometrically simple.

Evidence of retention of cluster nuclearity during reactions

To investigate whether the cluster frameworks changed during these transformations in the ligand sphere of the cluster, we recorded scanning transmission electron microscopy (STEM) images with an aberration-corrected instrument to determine the cluster sizes before and after reaction with O_2. The images (Figures 4 and S13 (ESI)) provide evidence of the heavy Ir atoms and show essentially no changes in average cluster framework diameter, 0.59 ± 0.12 nm before the treatment in O_2 and 0.60 ± 0.15 nm thereafter (the errors represent uncertainties in the measurements of the images, with the clusters being in various orientations with respect to the electron beam). The stable

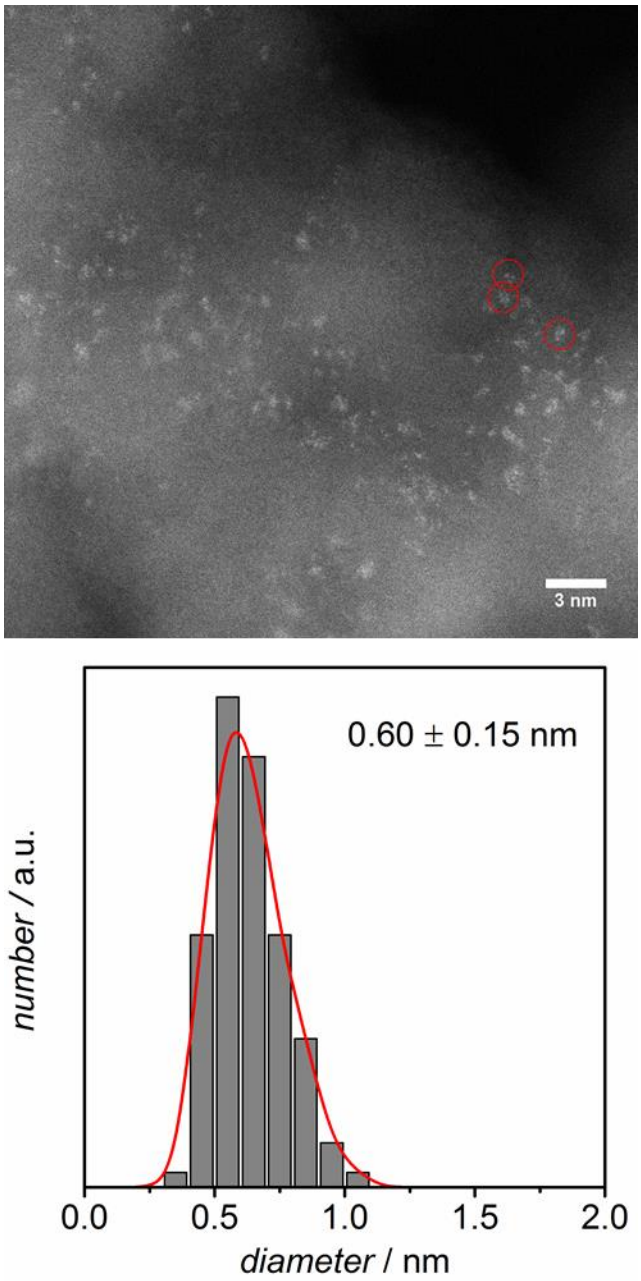

Figure 4. High angle annular dark field-STEM micrograph with histogram characterizing supported $Ir_4L_3(CO)_9$ clusters that had undergone 24 h of exposure to H_2 followed by 24 h of exposure to O_2 at 323 K and 1 bar.

cluster diameters after reaction with O_2 are consistent with reported diameters of other tetrairidium cluster frameworks.[43–45] We surmise that the steric bulk of the calixarene ligands preserves the structure of the Ir_4 framework, helping to avoid aggregation that could otherwise ensue during reaction with O_2. Such aggregation has been reported as being prevalent after oxidation of other silica-supported noble-metal clusters, which lack the protection afforded by the bulky ligands in our system.[46]

Demonstration that measured changes took place simultaneously.

The data demonstrate that numerous changes took place in the ligand sphere of the tetrairidium clusters during reactions investigated in this work. The plot of the characterization results shown in Figure 6 was constructed with infrared and X-

ray absorption spectroscopic data recorded as O_2 flowed (Reaction 2 in Figure 1). The data show that the changes indicated by the two spectroscopies took place in concert, characterizing the same changes in the clusters. Moreover, all of the data are internally consistent, with a common time scale of 27 min, and they are in agreement with the above-stated inference of the simple stoichiometry of the reaction. In the Discussion section, we evaluate possible structures in view of all the characterization data taken together.

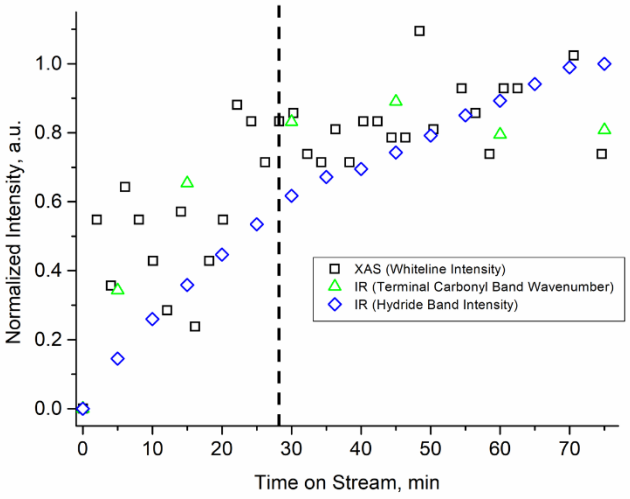

Figure 6. Changes in observed properties of supported tetrairidium clusters during exposure to O_2 at 323 K and 1 bar following incorporation of hydride ligands by exposure to H_2. Data are normalized as a magnitude of the fractional conversion to their respective steady state value. Details of sample preparation are provided in Figure 1 and in the text. The data demonstrate that all the changes took place simultaneously as characterized by the three different spectroscopic techniques.

Discussion

The key results are the following: (i) H_2 reacted with the silica-supported clusters as CO ligands were lost, and (ii) then O_2 reacted with the clusters to form oxygen-containing ligands. The carbonyl IR data characterizing the CO ligands that remained after O_2 treatment had the same wavenumbers as those in the original silica-supported $Ir_4L_3(CO)_9$ cluster. The gas-phase products of the reaction with O_2 included H_2 and not H_2O. These results raise the following questions: (1) What are the oxygen-containing ligands that formed on the clusters? (2) How many of these ligands were bonded to each cluster? (3) How was oxygen bonded to the metal framework, and how did it affect the electron density on the cluster core? (4) What do the data imply about the mechanism of formation of the oxygen-containing clusters? (5) What, if anything, is unique about the bonding of oxygen to these clusters? We address these questions below.

Identification of oxygen-containing ligands as peroxo.

Our assignment of a bridging peroxo species in **C2** at 756 cm^{-1} is supported by previously reported lower frequencies for such bands compared with mononuclear complexes,[30,32,47,48] and our observed frequency is in the range of frequencies observed for O-O vibrations assigned to bridging peroxo ligands, as reported for a number of complexes;[32–35,42] examples are complexes of iron, copper, cobalt, nickel, and platinum dimers. This range is more than 80 cm^{-1} lower in frequency compared with an η^2 peroxo O-O stretch (expected to occur at about 840 cm^{-1}; 885 cm^{-1} for atomic Ir).[6,7,10,11,51,52] In addition, this range is red shifted by more than 300 cm^{-1} relative to expectations for an Ir-OOH band (1100 cm^{-1}).[2] Many of the reported mononuclear iridium and rhodium complexes incorporating peroxo ligands incorporate η^2–peroxo ligands, but a dimeric iridium complex with a μ^1–η^1:η^1 peroxo ligand is specific to the work of Cowie (Figure 1),[27] whereas other dinuclear iridium species have been reported with a μ-oxo bridge between the two Ir atoms.[49,50]

We do not assign any significant O-O stretching character to the band at 788 cm^{-1} in Figures 5b, 5c, and 5e, based on the lack of shift of this band upon ^{18}O labelling, when comparing spectra for **C2** and **C3**. Instead, we infer that a similar change in symmetry as observed upon incorporating bridging peroxo ligands into **C1** when synthesizing **C2** and **C3**, also occurs after reacting **2** with O_2. This change of symmetry is accompanied by an increase in the change of polarizability, thereby enhancing the Raman signal in the vicinity of 788 cm^{-1} in Figures 5b, 5c, and 5e. Given the same 788 cm^{-1} band

that these three clusters share in common, and the 3 strongly donating phosphine ligands on the basal plane of cluster **2** (general electron richness of iridium basal plane), we thus rationalize similar bridging peroxo ligands as observed for **C2** and **C3** also in **2** following reaction with O_2. We discount formation of an Ir-OOH band, which could have possibly occured via O_2 insertion into the Ir-H bond of **2**, because new infrared bands in the spectral window of 3000 cm^{-1} – 3700 cm^{-1} would have been expected in this case upon reaction of the supported cluster with O_2, which was not observed (Figure S5, ESI). This lack of observed O_2 insertion into the Ir-H bond is consistent with results of Goldberg et al., who investigated the reaction of O_2 with Ir hydride pincer complexes, where such insertions were also not observed and instead bound peroxo ligands were formed.[53]

We stress that our IR spectra show a decrease in band areas corresponding to the total loss of two bridging carbonyls in **2**, sites that we hypothesize are occupied by the two peroxo species, as these bridging carbonyl sites were not repopulated with CO when the sample was exposed to CO (Figure S7, ESI) following reaction with O_2. This lack of recarbonylation indicates a strong and irreversible bonding of the postulated bridging dioxygen ligands persistently occupying the sites where bridging carbonyl ligands had been bonded originally, on the electron-rich basal plane (comprising substituted Ir atoms bound to phosphine ligands).[54–57] The electron richness of these substituted Ir atoms makes their chemistry distinct from that of the basal plane, as described previously to account for markedly increased rates of CO desorption.[38] The observed irreversibility of oxygen bonding is consistent with trends from prior electronic structure calculations, which correlate the strength of dioxygen bonding to the electron richness of metal clusters.[40,58–60]

Quantification and location of ligands on tetrairidium clusters.

During the sequence of reactions of the clusters summarized in Figure 1, the formation of hydride ligands on the clusters took place during the first exposure to flowing H_2, as shown by the hydride bands in the IR spectrum at 2110 cm^{-1}. A straightforward interpretation of the data is that the hydride ligands formed by the oxidative addition of H_2 to the cluster as CO ligands desorbed.[61,62] The 17 cm^{-1} shift in the frequency of a terminal CO band originally at 1994 cm^{-1} is a reflection of a depleted electronic charge on the cluster, as a result of incorporation of the hydride ligands[26]. We rule out cluster fragmentation and phosphine ligand oxidation, because in these cases, the IR spectra would have shown much more drastic changes. A blue shift in CO frequencies of more than 27 cm^{-1} would have been expected to be observed upon phosphine oxidation.[24] Instead, data in Figures 2a and 2b show that a red shift in the terminal CO band is observed upon reaction of the silica-supported cluster with O_2. This results in a terminal CO band frequency that is identical to the original silica-supported $Ir_4L_3(CO)_9$ cluster. We therefore ascribe the observed red shift to the loss of bound hydride ligands as H_2, as detected by mass spectrometry, and a lack of bound phosphine oxidation. This lack of phosphine oxidation is consistent with the general oxidative stability of phosphines bound to noble metals, as also observed by Strukul et al. when working with Pt(II) complexes incorporating phosphine ligands, in the presence of excess hydrogen peroxide.[63] Furthermore, the fragmentation of an Ir–Ir bond in the tetrahedral frame to synthesize a butterfly structure would have led to much greater spectral complexity than was observed, with new bands appearing and bands disappearing (frequencies and the symmetry of the IR bands in the CO region would have necessarily changed).[64,65]

Because these changes were reversed in a stoichiometrically simple reaction when the clusters were exposed to O_2, we infer that the formation of the bridging peroxo ligands took place concomitantly with the removal of hydride ligands. The mass spectra show that the latter were removed as H_2 but not water.

Reexposure of the clusters incorporating the peroxo ligands to H_2 again led to the formation of hydride ligands, again accompanied by changes in the carbonyl bands in the IR spectra reflective of the change in ligation. These changes were similar to those observed in the first exposure of the sample to H_2, but both the hydride band intensity and the extent of the blue shift of the CO band were significantly smaller—corresponding to about one-third of their original values in **2**. The inference we draw from the observation that the changes were only partial is that about 2/3 of the sites for hydride on the cluster were blocked by irreversibly bound bridging peroxo ligands.

We infer that these sites were located at the basal planes of the clusters, where electron-donating phosphine ligands are bonded, because, in earlier work, we showed that four basal-plane CO ligands per cluster were removed by exposure of the clusters to flowing H_2 at 333 K (and the process was reversible),[38] as well as the electron-richness of the substituted Ir atoms located there (vide supra).

The blocking of these basal-plane sites by peroxo ligands is consistent with the work on complexes in solution by Williams et al.,[66] who showed that peroxo ligands are difficult to remove from an iridium pincer complex at about room temperature in the presence of H_2 at 5 bar. Furthermore, in the presence of O_2 at 5 bar, no oxidation of the phosphine ligands was observed prior to the third day of treatment.[66] These findings are consistent with ours in showing the lack of oxygen reaction with the bound phosphine ligands and the retention of the peroxo ligands after a milder exposure to H_2

at 1 bar and 323 K. Indeed, bound phosphine ligands in noble-metal complexes have been shown to remain unreactive even under stronger oxidizing conditions involving 35% hydrogen peroxide.[63,67]

The carbonyl band wavenumbers after O_2 treatment are identical to those of silica-supported $Ir_4L_3(CO)_9$ (Figures 2a and b), and we therefore rule out the possibility of phosphine oxidation and confirm that all three phosphine ligands were retained. Were this not the case, large blue shifts (more than 27 cm^{-1}) would have been observed upon O_2 treatment, corresponding to CO band frequencies reported for $Ir_4L_1(CO)_{11}$, and $Ir_4L_2(CO)_{10}$.[24] The lack of a CO frequency shift resulting from the reaction with O_2 is an unexpected result, because oxidation of the metal core would be expected to cause a blue shift of these frequencies, which should be sensitive to the π-backbonding from the metal core to the CO ligands. A more electron-rich metal core should result in a greater degree of π*-backbonding to CO, which should be manifested in a red-shifted CO band (i.e., a weakening of the C-O bond as a result of electron density in the π-antibonding orbital).[24,68–72] Indeed, prior evidence of the bonding of peroxo ligands in organometallic complexes led to depletion of charge from the metal and thus to blue shifts in the ν_{CO} bands,[8,9] associated with the electron-withdrawing ability of the ligands complexed to metals.

Thus, we expected but did not observe shifts in the CO band frequencies of a decarbonylated variant of **2**, as a result of dative interaction between oxygen lone pairs and Ir atoms on the basis of a comparison of frequencies characterizing a similar decarbonylated cluster that was unsupported, in alkane solvent.[43] To explain the apparent anomaly, we surmise that competing phenomena compensated each other, disguising the expected effects.

On the basis of these results, we propose the structure of the supported clusters incorporating peroxo ligands as represented schematically in Figure 1.

Chemistry of reaction of O_2 with clusters.

The data indicate that the bridging peroxo ligands replaced hydride ligands that were removed as H_2, but this is only a simplified statement of the chemistry, because CO_2 also formed. Thus, we infer that hydride was not the only ligand to be removed in the reaction with O_2, and surmise that the oxygen was activated in a way that caused it to oxidize bound carbonyl ligands to make the observed CO_2. This interpretation is supported by the observed decrease in intensity of the terminal CO bands (Figure S1b, ESI). Such reactions of bound CO ligands have been commonly observed for metal carbonyls under various oxidizing conditions.[58–60,73] The quantitative data (Figure 1a and Table 1) indicate the loss of approximately one CO ligand per cluster during the reaction with O_2.

We wished to address whether a carbonato complex served as a detectable intermediate in the release of CO_2 during reaction with O_2. This could hypotheticaly occur via insertion of O_2 into a bound CO ligand. A related process involving insertion of CO into an peroxo ligand to synthesize an Ir-carbonato complex has been previously described.[53] We would expect such a complex to exhibit infrared bands around 1585 cm^{-1} and 1485 cm^{-1}.[41] However, our infrared data are inconsistent with the appearance of such bands during reaction with dioxygen, showing instead only slight changes in the region corresponding to the calixarene ligands, presumably as a result of incorporation of bound peroxo ligands (Figure S15 in the ESI). While we conclude that a carbonato complex as described above is not a stable intermediate, we cannot rule out that such a species could be a reactive intermediate preceding the loss of CO_2 formed below the detection limit of infrared spectroscopy.

To summarize, we infer reaction of O_2 with **2** pretreated with hydrogen gas flow removes bound hydride ligands as H_2, and one CO ligand per cluster is oxidized to form CO_2, as two bridging peroxo ligands form per cluster. Our results are contrasted with those reported for the reaction of a soluble iridium hydride pincer complex with O_2 to form water, which was observed by NMR spectroscopy. And we suggest that in that chemistry, H_2 might also have formed without being observed because of its low solubility in the C_6D_6 solution used in the experiments.[66]

Structure of tetrairidium clusters after reaction with O_2.

We emphasize that the lack of changes in the frequencies of the carbonyl bands in the IR spectra after incorporation of the peroxo ligands provides strong evidence that the tetrahedral cluster frame was preserved during reaction with O_2 (no breakage of an Ir–Ir bond to synthesize a butterfly cluster had occurred – *vide supra*. Aggregation of the iridium cluster is also ruled out on the basis of the STEM data (Figure S13, in the ESI).[46,74] We also rule out the formation of bulk iridium oxide; bulk noble metal oxides are known to be highly mobile on silica supports and aggregate to form large clusters that would have been visible by STEM. Furthermore, the lack of changes in the IR spectra demonstrate that no such massive changes in structure took place.[43–45]

Thus, we infer the structure of the supported tetrairidium cluster incorporating bridging peroxo ligands to be that shown schematically in Figure 1. We emphasize that the structural data are not precise enough to determine quite how

the cluster interacts with the silica support or how the support distorts the ligands on the cluster, but the approximate placement of the ligands is well supported by the data.

Conclusions

In summary, this is the first account of Raman characterization of bridging peroxo ligands on iridium, which formed under mild conditions involving the reaction of O_2. Uniquely, we surmise that the same ligands were bound to a silica-supported polyhedral metal cluster, without breaking of metal-metal bonds or reconstruction of the cluster framework. The results reported here for a tetrairidium cluster are consistent with these ligands being persistent in the presence of reducing and CO atmospheres, being anchored to the electron-rich basal plane where bulky phosphine ligands are bonded. We suggest that this peroxo-ligand synthesis chemistry may extend to iridium and perhaps other noble-metal metal surfaces, and the results may have significant implications for catalysis on metal surfaces.

Experimental Methods

Sample Handling and Preparation of Silica Supported $Ir_4L_3(CO)_9$

Aerosil 200 was refluxed with nanopure water overnight. The slurry was cooled to room temperature and centrifuged and the water phase was decanted and the solid dried at 473 K. The dried silica was ground into a fine powder and calcined with dry air (100 mL/min) and argon (50 mL/min) at 773 K. The BET surface area of the calcined silica was 190 ± 3 m^2/g.

With standard air-exclusion techniques, $Ir_4L_3(CO)_9$ (synthesized as reported elsewhere[24]) was adsorbed on partially dehydroxylated silica, as the mixtures was slurried with distilled *n*-hexane (dried with sodium hydride). The solution color quickly changed from yellow to colourless, indicating complete uptake of the cluster by the support. The solvent was removed by evacuation (pressure = 150 mTorr), yielding a sample containing 1.0 wt% iridium. IR spectra of the solution and of the material formed by adsorbing the iridium complex on silica are reported elsewhere;[38] the spectrum of the iridium species remained essentially unchanged upon adsorption, as expected. Samples were stored in an argon-filled glovebox (O_2 and H_2O monitor readings < 5 ppm). All samples were handled using standard air-exclusion techniques.

In-situ Fourier Transform Infrared Spectroscopy

A Nicolet 6700 FTIR spectrometer with a spectral resolution of 2 cm^{-1} was used to collect transmission IR spectra of catalyst samples. Approximately 30 mg of solid powder sample was pressed into a thin wafer and loaded into an *in-situ* IR flow cell equipped with CaF_2 windows (In-situ Research Institute) in the glovebox. The sample wafer could be heated, and its temperature was monitored with a K-type thermocouple. Each spectrum represents the average of 64 scans.

Mass Spectrometry

Mass spectra were measured with a Balzers OmniStar mass spectrometer running in multi-ion monitoring mode. Changes in signals were observed for H_2 (*m/z* = 2), HD (*m/z* = 3), H_2O (*m/z* = 18), and CO_2 (*m/z* = 44). Measurements of silica-supported clusters that has been exposed to flowing gases were carried out by measuring the off-gas from a reactor that had been loaded in the glovebox.

FT-Raman Spectroscopy

Experiments were done with a Bruker IFS66 V instrument equipped with a FRA-106 Raman accessory. Spectra of powder samples were measured in a sealed quartz tube (the samples were **2**; **2** after $H_2/^{16}O_2$ or $H_2/^{18}O_2$ treatment; **C2** synthesized by exposure to $^{18}O_2$; silica, as a control) or in a windowless metal holder (**C1** and **C2** synthesized by exposure to $^{16}O_2$) at a 4 cm^{-1} resolution. Conditions: 175 mW, 1064 nm Nd:Yag laser radiation, 2000-10000 scans. Samples of silica-supported tetrairidium clusters reacting with $^{16}O_2$ were synthesized in flowing O_2 for 20 h at 50 °C or in static $^{18}O_2$ in the headspace of a batch reactor, for a period of 2 h at 50 °C. The latter synthesis procedure was required because of the limited availability of $^{18}O_2$.

X-ray Absorption Spectroscopy

Samples were exposed to the same conditions as stated for the IR experiments. X-ray absorption spectra were recorded at X-ray beamline 10-ID at the Argonne Photon Source (APS). A Si (220) monochromator was tuned to the maximum intensity at the Ir L_{III} edge. In an argon-filled glovebox, each sample was pressed into a wafer, mounted in a cell.[75] The mass of each sample (approximately 0.25 g) was chosen to give an absorbance of 2.5 calculated at 50 eV above the absorption edge (11210 eV). Spectra were collected in transmission mode by use of ion chambers mounted on each end of the sample cell. For calibration purposes, measurement of the absorption of a platinum foil, placed downbeam of the sample, was carried out simultaneously.

Scanning Transmission Electron Microscopy

High-angle annular dark-field scanning transmission electron microscopy (HAADF-STEM) was conducted with a modified, double aberration-corrected FEI Titan 80-300 microscope operating at 300 kV. Samples suitable for HAADF-STEM were prepared on Ted Pella amorphous lacey-carbon films on copper grids in a glovebox. Average cluster diameters were calculated by statistical evaluation of at least 100 clusters on HAADF-STEM images using Image J 1.47v software.

Computational Methods

The geometry optimization of the clusters was performed using DFT with ωB97X-D,[76] a hybrid functional with long-range and dispersion corrections. For the light elements, we used the DZVP2 polarized double-zeta basis set[77] and a relativistic pseudopotential correlation consistent double-zeta cc-pVDZ-pp basis set for iridium.[78] The PP on Ir includes 60 electrons, $1s^2 2s^2 2p^6 3s^2 3p^6 3d^{10} 4s^2 4p^6 4d^{10} 4f^{14}$, with 17 electrons $5s^2 5p^6 6s^2 5d^7$ included in the self-consistent field calculations. All calculations were performed with the Gaussian09 suite of programs.[79]

Acknowledgements

The characterization aspects of this work were supported by the U.S. Department of Energy, Office of Science, Basic Energy Sciences (DE-FG02-04ER15513 (AP) and DE-FG02-05ER15696), while the syntheses were supported by the Management and Transfer of Hydrogen via Catalysis Program funded by Chevron Corporation. All microscopy work was performed at the Molecular Foundry and was supported by the Office of Science, Office of Basic Energy Sciences, of the U.S. Department of Energy under Contract No. DE-AC02-05CH11231. Computational work at the University of Alabama was supported by a subcontract from Pacific Northwest National Laboratory (KC0301050-47319). C. S. acknowledges the Deutsche Forschungs-gemeinschaft (DFG) for a research fellowship. DAD also thanks the Robert Ramsay Chair Fund of The University of Alabama for support.

References

1 J. C. Goloboy and W. G. Klemperer, *Angew. Chem. Int. Ed.*, 2009, **48**, 3562–3564.
2 P. L. Holland, *Dalt. Trans.*, 2010, **39**, 5415.
3 G. Henrici-Olivé and S. Olivé, *Angew. Chemie Int. Ed.*, 1974, **13**, 29–38.
4 J. S. Valentine, *Chem. Rev.*, 1973, **73**, 235–245.
5 J. Cipot-Wechsler, D. Covelli, J. M. Praetorius, N. Hearns, O. V. Zenkina, E. C. Keske, R. Wang, P. Kennepohl and C. M. Crudden, *Organometallics*, 2012, **31**, 7306–7315.
6 H. F. Haarman, F. R. Bregman, P. W. N. M. van Leeuwen and K. Vrieze, *Organometallics*, 1997, **16**, 979–985.
7 X. Y. Yu, B. O. Patrick and B. R. James, *Organometallics*, 2006, **25**, 4870–4877.
8 M. Selke, L. Rosenberg, J. M. Salvo and C. S. Foote, *Inorg. Chem.*, 1996, **35**, 4519–4522.
9 C. J. Huber, T. C. Anglin, B. H. Jones, N. Muthu, C. J. Cramer and A. M. Massari, *J. Phys. Chem. A*, 2012, **116**, 9279–9286.
10 M. A. Ciriano, J. A. López, L. A. Oro, J. J. Pérez-Torrente, M. Lanfranchi, A. Tiripicchio and M. T. Camellini, *Organometallics*, 1995, **14**, 4764–4775.
11 H. Lebel, C. Ladjel, F. Bélanger-Gariépy and F. Schaper, *J. Organomet. Chem.*, 2008, **693**, 2645–2648.
12 P. Pareja, A. Amariglio and H. Amariglio, *J. Catal.*, 1975, **36**, 379–384.
13 I. Önal and J. B. Butt, *J. Chem. Soc., Faraday Trans. 1*, 1982, **78**, 1887–1898.

14 B. Delmon and G. F. Froment, *Catal. Rev.*, 1996, **38**, 69–100.
15 F. Ribeiro, M. Boudart, R. Dalla Betta and E. Iglesia, *J. Catal.*, 1991, **130**, 498–513.
16 G. H. Twigg and E. K. Rideal, *Trans. Faraday Soc.*, 1940, **35**, 533–537.
17 Z. Huang, P. S. White and M. Brookhart, *Nature*, 2010, **465**, 598–601.
18 S. Yamazoe, K. Koyasu and T. Tsukuda, *Acc. Chem. Res.*, 2014, **47**, 816–824.
19 J. Saavedra, H. A. Doan, C. J. Pursell, L. C. Grabow and B. D. Chandler, *Science*, 2014, **345**, 1599–1602.
20 J. Zhao and R. Jin, *Nano Today*, 2018, **18**, 86–102.
21 T. Ward, L. Delannoy, R. Hahn, S. Kendell, C. J. Pursell, C. Louis and B. D. Chandler, *ACS Catal.*, 2013, **3**, 2644–2653.
22 H. Lang, S. Maldonado, K. J. Stevenson and B. D. Chandler, *J. Am. Chem. Soc.*, 2004, **126**, 12949–12956.
23 M. Yang, S. Li, Y. Wang, J. A. Herron, Y. Xu, L. F. Allard, S. Lee, J. Huang, M. Mavrikakis and M. Flytzani-Stephanopoulos, *Science*, 2014, **346**, 1498–1501.
24 A. Okrut, O. Gazit, N. De Silva, R. Nichiporuk, A. Solovyov and A. Katz, *Dalt. Trans.*, 2012, **41**, 2091.
25 B. C. Gates, M. Flytzani-Stephanopoulos, D. A. Dixon and A. Katz, *Catal. Sci. Technol.*, 2017, **7**, 4259–4275.
26 A. P. Palermo, S. Zhang, S. Hwang and D. A. Dixon, *Dalt. Trans.*, 2018.
27 J. Xiao, B. D. Santarsiero, B. A. Vaartstra and M. Cowie, *J. Amer*, 1993, **2**, 3212–3220.
28 B. A. Vaartstra, J. Xiao, J. A. Jenkins, R. Verhagen and M. Cowie, *Organometallics*, 1991, **10**, 2708–2717.
29 I. Shweky, L. E. Pence, G. C. Papaefthymiou, R. Sessoli, J. W. Yun, A. Bino and S. J. Lippard, *J. Am. Chem. Soc.*, 1997, **119**, 1037–1042.
30 M. J. Henson, M. A. Vance, C. X. Zhang, H.-C. Liang, K. D. Karlin and E. I. Solomon, *J. Am. Chem. Soc.*, 2003, **125**, 5186–5192.
31 L. Q. Hatcher, M. A. Vance, A. A. N. Sarjeant, E. I. Solomon and K. D. Karlin, *Inorg. Chem.*, 2006, **45**, 3004–3013.
32 Z. Gao, H. Kim, Q. Sun, P. C. Stair and W. M. H. Sachtler, *J. Phys. Chem. B*, 2001, **105**, 6186–6190.
33 D. Ramprasad, A. G. Gilicinski, T. J. Markley and G. P. Pez, *Inorg. Chem.*, 1994, **33**, 2841–2847.
34 M. S. Davies and T. W. Hambley, *Inorg. Chem.*, 1998, **37**, 5408–5409.
35 K. D. Karlin, S. Kaderli and A. D. Zuberbühler, *Acc. Chem. Res.*, 1997, **30**, 139–147.
36 G. C. Wang, H. H. Y. Sung, I. D. Williams and W. H. Leung, *Inorg. Chem.*, 2012, **51**, 3640–3647.
37 M. Feller, E. Ben-Ari, Y. Diskin-Posner, R. Carmieli, L. Weiner and D. Milstein, *J. Am. Chem. Soc.*, 2015, **137**, 4634–4637.
38 A. Palermo, A. Solovyov, D. Ertler, A. Okrut and B. C. Gates, *Chem. Sci.*, 2017, **8**, 4951–4960.
39 O. Lopez-Acevedo, K. A. Kacprzak, J. Akola and H. Häkkinen, *Nat. Chem.*, 2010, **2**, 329–334.
40 X. Chen and H. Häkkinen, *J. Am. Chem. Soc.*, 2013, **135**, 12944–12947.
41 B. J. Tickner, W. Lali, S. S. Roy, A. C. Whitwood and S. B. Duckett, *ChemPhysChem*, 2018.
42 P.-C. Duan, D.-H. Manz, S. Dechert, S. Demeshko and F. Meyer, *J. Am. Chem. Soc.*, 2018, **140**, 4929–4939.
43 A. Okrut, R. C. Runnebaum, X. Ouyang, J. Lu, C. Aydin, S.-J. Hwang, S. Zhang, O. A. Olatunji-Ojo, K. A. Durkin, D. A. Dixon, B. C. Gates and A. Katz, *Nat. Nanotechnol.*, 2014, **9**, 459–465.
44 D. Braga, F. Grepioni, J. J. Byrne and M. J. Calhorda, *J. Chem. Soc. Dalt. Trans. Inorg. Chem.*, 1995, 3287–3296.
45 J. Lu, P. Serna, C. Aydin, N. D. Browning and B. C. Gates, *J. Am. Chem. Soc.*, 2011, **133**, 16186–16195.
46 S. Soled, *Science*, 2015, **350**, 1171–1172.
47 Y. Funahashi, T. Nishikawa, Y. Wasada-Tsutsui, Y. Kajita, S. Yamaguchi, H. Arii, T. Ozawa, K. Jitsukawa, T. Tosha, S. Hirota, T. Kitagawa and H. Masuda, *J. Am. Chem. Soc.*, 2008, **130**, 16444–16445.
48 E. I. Solomon, P. Chen, M. Metz, S.-K. Lee and A. E. Palmer, *Angew. Chemie Int. Ed.*, 2001, **40**, 4570–4590.
49 Y. Zhao, X. Yan, K. R. Yang, S. Cao, Q. Dong, J. E. Thorne, K. L. Materna, S. Zhu, X. Pan, M. Flytzani-Stephanopoulos, G. W. Brudvig, V. S. Batista and D. Wang, *ACS Cent. Sci.*, 2018, 1166–1172.
50 Y. Zhao, K. R. Yang, Z. Wang, X. Yan, S. Cao, Y. Ye, Q. Dong, X. Zhang, J. E. Thorne, L. Jin, K. L. Materna, A. Trimpalis, H. Bai, S. C. Fakra, X. Zhong, P. Wang, X. Pan, J. Guo, M. Flytzani-Stephanopoulos, G. W. Brudvig, V. S. Batista and D. Wang, *PNAS*, 2018, **115**, 2902–2907.
51 J. E. Molinari and I. E. Wachs, *J. Am. Chem. Soc.*, 2010, **132**, 12559–12561.
52 D. K. Dutta, B. Deb, B. J. Sarmah, J. D. Woollins, A. M. Z. Slawin, A. L. Fuller and R. A. M. Randall, *Eur. J. Inorg. Chem.*, 2011, **2011**, 835–841.
53 L. Boisvert and K. I. Goldberg, *Acc. Chem. Res.*, 2012, **45**, 899–910.
54 B. F. G. Johnson and Y. V. Roberts, *Inorg. Chim. Acta*, 1993, **205**, 175–179.
55 D. C. Sonnenberger and J. D. Atwood, *Organometallics*, 1982, **1**, 694–698.
56 D. C. Sonnenberger and J. D. Atwood, *J. Am. Chem. Soc.*, 1982, **104**, 2113–2116.
57 K. J. Karel and J. R.Norton, *J. Am. Chem. Soc.*, 1974, **96**, 6812–6813.
58 N. Lopez, T. V. W. Janssens, B. S. Clausen, Y. Xu, M. Mavrikakis, T. Bligaard and J. K. Nørskov, *J. Catal.*, 2004, **223**, 232–

235.
59 Y. P. G. Chua, G. T. K. K. Gunasooriya, M. Saeys and E. G. Seebauer, *J. Catal.*, 2014, **311**, 306–313.
60 I. X. Green, W. Tang, M. McEntee, M. Neurock and J. T. Yates, *J. Am. Chem. Soc.*, 2012, **134**, 12717–12723.
61 L. Vaska and J. W. DiLuzio, *J. Am. Chem. Soc.*, 1962, **84**, 679–680.
62 J. P. Collman, *J. Am. Chem. Soc.*, 1968, **1**, 136–143.
63 M. Colladon, A. Scarso, P. Sgarbossa, R. A. Michelin and G. Strukul, *J. Am. Chem. Soc.*, 2007, **129**, 7680–7689.
64 L. Malatesta and G. Caglio, *Chem. Commun.*, 1967, 420–421.
65 B. K. Park, M. A. Miah, G. Lee, Y. J. Cho, K. Lee, S. Park, M. G. Choi and J. T. Park, *Angew. Chemie - Int. Ed.*, 2004, **43**, 1712–1714.
66 D. B. Williams, W. Kaminsky, J. M. Mayer and K. I. Goldberg, *Chem. Commun.*, 2008, **3**, 4195.
67 A. Cavarzan, A. Scarso, P. Sgarbossa, R. A. Michelin and G. Strukul, *ChemCatChem*, 2010, **2**, 1296–1302.
68 C. Li and Y. Liu, in *Bridging Heterogeneous and Homogeneous Catalysis: Concepts, Strategies, and Applications*, Wiley-VCH, Weinheim, 2014, pp. 325–350.
69 G. Blyholder, *J. Phys. Chem.*, 1964, **68**, 2772–2777.
70 A. Fielicke, G. Von Helden, G. Meijer, D. B. Pedersen, B. Simard and D. M. Rayner, *J. Chem. Phys.*, 2006, **124**.
71 C. A. Tolman, *J. Am. Chem. Soc.*, 1970, **92**, 2953–2956.
72 C. A. Tolman, *J. Am. Chem. Soc.*, 1970, **92**, 2956–2965.
73 J. D. Henao, T. Caputo, J. H. Yang, M. C. Kung and H. H. Kung, *J. Phys. Chem. B*, 2006, **110**, 8689–8700.
74 O. S. Alexeev, F. Li, M. D. Amiridis and B. C. Gates, *J. Phys. Chem. B*, 2005, **109**, 2338–2349.
75 R. E. Jentoft, S. E. Deutsch and B. C. Gates, *Rev. Sci. Sintrum.*, 1996, **67**, 2111–2112.
76 J. Chai and M. Head-Gordon, *Phys. Chem. Chem. Phys.*, 2008, **10**, 6615–6620.
77 N. Godbout, D. Salahub, J. Andzelm and E. Wimmer, *Can. J. Chem.*, 1992, **70**, 560–571.
78 D. Figgen, K. A. Peterson, M. Dolg and H. Stoll, *J. Chem. Phys.*, 2009, **130**, 164108–1 – 164108–12.
79 M. J. Frisch, G. W. Trucks, H. B. Schlegel, G. E. Scuseria, M. A. Robb, J. R. Cheeseman, G. Scalmani, V. Barone, B. Mennucci, G. A. Petersson, H. Nakatsuji, M. Caricato, X. Li, H. P. Hratchian, A. F. Izmaylov, J. Bloino, G. Zheng, J. L. Sonnenberg, M. Hada, M. Ehara, K. Toyota, R. Fukuda, J. Hasegawa, M. Ishida, T. Nakajima, Y. Honda, O. Kitao, H. Nakai, T. Vreven, J. A. Montgomery Jr., J. E. Peralta, F. Ogliaro, M. Bearpark, J. J. Heyd, E. Brothers, K. N. Kudin, V. N. Staroverov, R. Kobayashi, J. Normand, K. Raghavachari, A. Rendell, J. C. Burant, S. S. Iyengar, J. Tomasi, M. Cossi, N. Rega, J. M. Millam, M. Klene, J. E. Knox, J. B. Cross, V. Bakken, C. Adamo, J. Jaramillo, R. Gomperts, R. E. Stratmann, O. Yazyev, A. J. Austin, R. Cammi, C. Pomelli, J. W. Ochterski, R. L. Martin, K. Morokuma, V. G. Zakrzewski, G. A. Voth, P. Salvador, J. J. Dannenberg, S. Dapprich, A. D. Daniels, Ö. Farkas, J. B. Foresman, J. V. Ortiz, J. Cioslowski and D. J. Fox, 2009.